Use of an Ion-exchange Adduct of Synthetic Hectorite and Chiral Copper(II) Complex as a Packing Material for Chromatographic Resolution

Akihiko Yamagishi,[a] *Kenji Tamura,**[b] *Masumi Kamon,*[b] *Jun Yoshida* [c] *and Hisako Sato**[d]

[a] Toho University, School of Medicine, Ohta-ku, Tokyo 143-8540, Japan

[b] National Institute for Materials Science, Environmental Circulation Composite Materials Group, Tsukuba, 305-0044, Japan

[c] Nihon University, Department of Chemistry, College of Humanities & Sciences, Setagaya-ku, Tokyo 156-8550, Japan

[d] Ehime University, Department of Chemistry, College of Science, Matsuyama, Ehime 790-8577, Japan,

*Corresponding author: Kenji Tamura (TAMURA.Kenji@nims.go.jp)

Tel: +81-29-860-4370, Fax: +81-29-860-4667

Abstract

A spherically shaped particle of synthetic hectorite (denoted as Na-HEC) was ion-exchanged with a divalent Cu(II) complex, $[Cu(SS\text{-oxa})]^{2+}$ (*SS*-oxa = *SS*-2,2′-isopropylidene-bis(4-phenyl-2-oxazoline)). The material is denoted as $[Cu(SS\text{-oxa})]^{2+}$/HEC. A column for high performance liquid chromatography (HPLC) was prepared by packing 4.0 g of $[Cu(SS\text{-oxa})]^{2+}$/HEC into a stainless tube (25 cm x 0.4 cm (i.d.)). When tris(acetylacetonato)cobalt(III) (denoted as $[Co(acac)_3]$) was eluted by methanol at the flow rate of 0.2 $mLmin^{-1}$ and 4 ^oC, the compound was separated to Δ- and Λ-enantiomers nearly to the baseline separation. Organic molecules with two hydroxyl groups such as 1,1'-binaphthyl-2,2'-diol were also resolved partially. The results promised the practical utility of the clay column chromatography for obtaining enantiomeric compounds.

Keywords: Ion-exchange adducts; synthetic hectorite; chiral copper(II) complexes; high performance liquid chromatograph; optical resolution

1. Introduction

A smectite clay mineral exhibits unique characters when it adsorbs cationic species (Ogawa and Kuroda, 1995; Shichi and Takagi, 2000; Schoonhedyt, 2014). As a two-dimensional adsorbent, the clay mineral binds a cationic species either on the external surfaces or in the interlayer. A layer is charged negatively due to the isomorphous substitution of Si(IV) or Al(III) by lower valent metal ions. A negatively charged sites exists at high surface density (c. a. one negative charge (e^-) per 100 nm^2). Moreover, the external surface of a layer is characterized by the two-dimensional periodicity of phyllosilicate networks. Owing to these characters, an adsorbed molecule exhibits the following unique features: (i) it takes uniform orientation with respect to a layer surface and (ii) it is arranged under two-dimensional regularity.

From the viewpoint of molecular recognition, the above features ((i) and (ii)) lead to the hypothesis that a pre-adsorbed molecule interacts with an approaching molecule, recognizing its shape in cooperative manners. In case that a pre-adsorbed molecule is chiral, it may interact in stereoselective manners (Yoshida et al., 2020a, 2020b; Sato et al. 2018a, 2018b; Yamagishi and Sato, 2012; Kotkar and Ghosh, 1987). Prompted by this view, we developed clay column chromatography for optical resolution (Yamagishi et al., 2022, 2021, 2012, 1996, 1992; Yamagishi, 1986,1985,1981; Yamagishi and Ohnishi, 1982; Kakegawa and Yamagishi, 2006; Okada et al., 2018). In the attempts, an ion-exchange adduct of a smectite clay mineral and a chiral cationic molecule was prepared. The substance was used as a packing material of a column in liquid chromatography. When a chiral molecule is eluted through the column, it may interact with the pre-adsorbed chiral metal complex stereoselectively. The interactions affect the rate of elution,

66 depending on the chirality relation between pre-adsorbed and eluted molecules.
67 Accordingly the opposite enantiomers are eluted at different elution volumes to achieve
68 optical resolution. As a successful example, the column packed with an ion-exchange
69 adduct of Δ- or Λ-$[Ru(phen)_3]^{2+}$ (phen = 1, 10-pehnanthroline) and a synthetic hectorite
70 was proved to resolve a wide scope of inorganic and organic chiral molecules (Yamagishi
71 and Sato, 2012). Since a smectite clay mineral itself is achiral, a pre-adsorbed chiral
72 molecule (e. g. Δ- or Λ-$[Ru(phen)_3]^{2+}$) is denoted as a "*chiral director"*. The column is
73 stable at high temperature (> 30 °C) for a long time and exhibits high separation capacity
74 in comparison to the known commercially available chiral columns. The mechanism of
75 chiral recognition was revealed by vibrational circular dichroism spectroscopy (Sato et
76 al., 2022, 2018a, 2018b).

77 In the present work, a column was developed using a chiral copper(II) as a *chiral*
78 *director*. The used complex was $[Cu(SS\text{-oxa})]^{2+}$ (*SS*-oxa = 2,2′-isopropylidene-bis(4-
79 phenyl-2-oxazoline)). The complex is known to act as a homogeneous asymmetric
80 catalyst for various organic reactions (Johnson et al., 2000). Moreover, there is a report
81 that the complex is immobilized in a smectite clay mineral and employed as a
82 heterogeneous asymmetric catalyst (Fraile et al., 2009; Sato, et al., 2021). An adduct was
83 prepared by ion-exchanging synthetic hectorite with $[Cu(SS\text{-oxa})]^{2+}$. Using the column
84 packed with the ion-exchange adduct, optical resolution was attempted by eluting a
85 racemic mixture of tris(acetylacetonato)cobalt(III) (denoted as $[Co(acac)_3]$) by methanol.
86 As a result, a racemic mixture of $[Co(acac)_3]$ was separated to Δ- and Λ-enantiomers
87 nearly completely. The mechanism of resolution was investigated by the theoretical
88 simulations. The same column resolved partially an organic molecule with two hydroxyl

groups such as 1,1'-binaphthyl-2,2'-diol (denoted as BINAL). The results promised the practical utility of the present column for obtaining enantiomeric inorganic and organic compounds chromatographically.

2. Experimental

2.1. Materials: *S,S*-2,2'-(dimethylmethylene)bis(4-phenyl-2-oxazoline) (denoted as *S,S*-oxa), copper(II)trifluoromethanesulfonate (denoted as $[Cu(TFMS)_2]$), dibenzoylmethane (denoted as dbmH), racemic tris(acetyacetonato)metal(III) (denoted as $[M(acac)_3]$: M = Co, Cr, Ru, Ir and Rh), 1,1'-binaphthyl-2, 2'-diol (denoted as BINAL), *R*- and *S*-phenylethane-1, 2-diol, racemic 1-phenylethanol, racemic 1-phenylethyamine and *SS*- and *RR*-1, 2-diphenylethane-1, 2-diols were purchased from Tokyo Kasei Co. Ltd. (Japan) and used as received. 1,1'-binaphthyl-2, 2'-dibromomethoxy (denoted as BINAL-Br) was synthesized in our laboratory. As shown in Fig. S1, the purity of the compound was confirmed by being eluted on a chiral column (RU-1 Ceramosphere, Shiseido Co. Ltd. Japan). Used methanol was of reagent (Tokyo Kasei Co. Ltd. (Japan)).

Synthetic hectorite (Laponite RD; denoted as Na-HEC) was purchased from BYK Additives & Instruments (U. K.). Its elemental composition and cation exchange capacity (CEC) are stated to be $(Na_{0.37}Ca_{0.01})[(Mg_{2.80}Li_{0.19})(Si_{3.96}O_{10})(OH)_2]$ and 0.65 milli-equivalents per gram, respectively. The spherical particle of Na-HEC (c.a. 5 μm in averaged diameter) was prepared by the spray-drying method as described previously (Sakuma et al., 2018). The specific surface area and pore volume for the spherical particle were estimated by nitrogen adsorption−desorption isotherms (Fig. S2, Table. S1).

2.2 Instrument: The prepared clay particles were characterized using XRD (Rigaku

112 Ultima IV) with Cu Kα radiation (λ = 0.15418 nm) under conditions of 40 kV and 30 mA,
113 and at scanning rate of 2 °/min. Surfaces of the clay particles were observed by scanning
114 electron microscopy (Quanta 600 SEM, FEI). The surface areas of the samples were also
115 estimated from nitrogen adsorption measurements (BELSORP-max, MicrotracBEL
116 Corp.). UV-visible electronic spectra were recorded using a UV–vis spectrophotometer
117 (U-2810, Hitachi Ltd., Japan). Electronic circular dichroism (ECD) spectra were
118 measured using a polarimeter (J-720, JASCO Corporation, Japan). High performance
119 liquid chromatography (HPLC) was performed using a Gulliver HPLC system (JASCO,
120 Japan). For checking the purity of a used compound, a commercial column
121 (Ceramosphere RU-1 (SHISEIDO, Japan)) was used.
122 ***2.3 Preparation of a chiral clay column:*** [Cu(*SS*-oxa)](TFMS)$_2$ was prepared by mixing
123 equimolar amounts of copper(II) trifluoromethanesulfonate (or [Cu(TFMS)$_2$]) and *SS*-
124 2,2'-isopropylidene-bis(4-phenyl-2-oxazoline) (or *SS*-oxa) in methanol. [Cu(*SS*-
125 oxa)(dbm)](TFMS) was prepared by mixing equimolar amounts of [Cu(*SS*-oxa)](TFMS)
126 and dbmH in methanol. The preparation and identification of [Cu(*SS*-oxa)(dbm)](TFMS)
127 was described elsewhere (Sato et al., 2020). The progresses of these reactions were
128 monitored by the change of UV-vis spectra.
129 For preparing a column, 3.3 g of the spherical particles of Na-HEC was dispersed in
130 50 mL of methanol. A methanol solution containing 1.9×10^{-3} mole of [Cu(*SS*-
131 oxa)](TFMS)$_2$ was added slowly under stirring. The clay particle was coloured blue,
132 indicating that [Cu(*SS*-oxa)]$^{2+}$ was ion-exchanged with Na^+ ion in Na-HEC spontaneously.
133 The resultant material was denoted as [Cu(*SS*-oxa)]$^{2+}$/HEC. After filtering the suspension,
134 the solid precipitate or [Cu(*SS*-oxa)]$^{2+}$/HEC (4.0 g) was dried under air. 4.0g of [Cu(*SS*-

oxa)]$^{2+}$/HEC was packed into a stainless tube (25 cm × 4 mm (i.d.)). XRD patterns and SEM images were measured before and after the ion-exchanging of Na-HEC particles with [Cu(*SS*-oxa)]$^{2+}$ (Figs. S3 and S4). The dead volume (V_d) of the column was determined to be 1.67 mL by eluting 10 μL of chloroform. In the similar way, a column of [Cu(*SS*-oxa)(dbm)]$^{+}$/HEC (5 cm × 0.4 cm (i.d.)) was prepared. Its V_d was determined to be 0.52 mL.

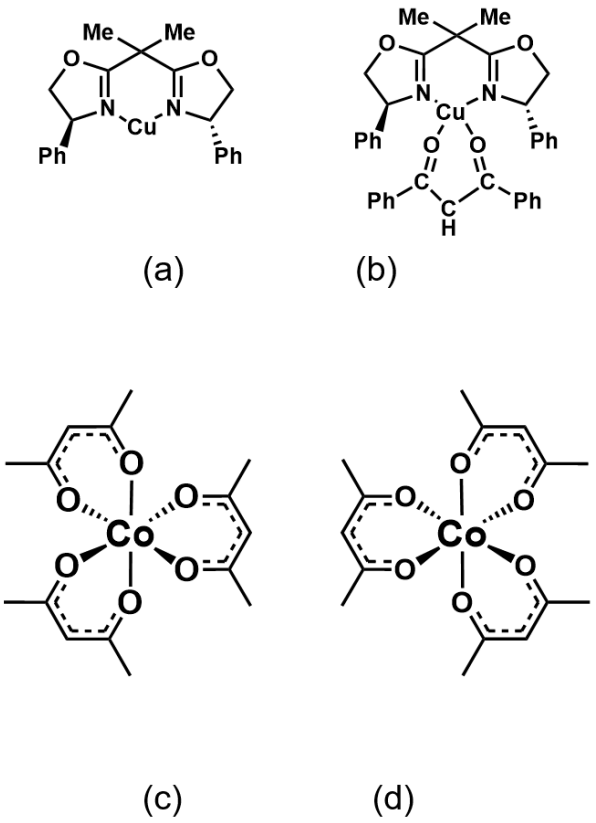

Chart 1. Molecular structures of (a) [Cu(*SS*-oxa)]$^{2+}$, (b) [Cu(*SS*-oxa)(dbm)]$^{+}$, (c) Λ-[Co(acac)$_3$] and (d) Δ-[Co(acac)$_3$].

2.4 Computational methods: The association structure between [Cu(*SS*-oxa)]$^{2+}$ and [Ru(acac)$_3$] was investigated by the theoretical simulation. The method was based on the dynamic DFT calculation. The same approach has been taken previously in several examples to study the details of intermolecular interaction of a resolved molecule and a chiral director fixed on a solid surface (Sato et al., 2020; Sato et al., 2021; Yamagishi et al., 2021; Yamagishi et al., 2022). The calculation was made for the association model between [Cu(*SS*-oxa)]$^{2+}$ and Δ- or Λ-[Co(acac)$_3$]. Gaussian 16 program (C.02) was used (Frisch et al., 2019). Geometry optimization was performed at the DFT (Density Functional Theory) at the level of 6-31G (d,p.) for all atoms. For an intercalation model, the upper and lower clay layers were replaced with a SiO_4^{2-} anion. At the initial optimization, the anion was fixed, and the other was positionally optimized. After convergence, the positions of all the molecules were freely moved for optimization. Finally geometry optimization was performed at the DFT-d3 (Density Functional Theory and empirical dispersion) at the level of 6-31G (d,p.) for all atoms.

Results and Discussion

3.1. ***Resolution of racemic tris(acetylacetonato)cobalt(III):*** For examining the resolution capability of the prepared [Cu(*SS*-oxa)]$^{2+}$/HEC column, racemic tris(acetylacetonato)cobalt(III) (denoted as [Co(acac)$_3$]) was eluted by methanol. [Co(acac)$_3$] is neutral and possesses a nearly spherical shape. Chirality arises from the helical twisting of three acetyacetonato (denoted by acac$^-$) ligands around a central Co(III) ion (Chart 1). Its helicity is denoted as ΔΔΔ or (simply as Δ) or ΛΛΛ (simply as Λ),

168 depending on the twisting direction. Since the molecule possesses no functional group on
169 the outer surface, it is difficult to be optically resolved by use of resolving reagents such
170 as camphor or tartaric acid. The enantiomer is stable against racemization at room
171 temperature. In case that the molecule is resolved on a chiral column, it indicates that
172 there exists a microscopic cavity in a column material to recognize the asymmetric
173 structure of an eluted molecule.

174 Curve (A) in Figure 1 shows the chromatogram when [$Co(acac)_3$] (1×10^{-8} mole)
175 was eluted at 4℃ and the flow rate of 0.2 mLmin^{-}1. Two peaks were obtained nearly on
176 the baseline separation. Collecting an eluted solvent at the first and second peaks, their
177 electronic circular dichroism (ECD) spectra were measured. It was concluded that the
178 first and second bands corresponded to the Δ- and Λ-enantiomers of [$Co(acac)_3$],
179 respectively. The elution order was also confirmed by flowing Δ- and Λ-enantiomers
180 separately. The separation factor (α) was given by

181 $$\alpha = (V_2-V_d)/(V_1-V_d) \qquad (1)$$

182 in which V_1, V_2 and V_d were the elution volumes of the less and more retained peaks and
183 the dead volume (1.67 mL), respectively. The value of α was calculated to be 1.11. The
184 value was comparable to those of commercially available columns (e.g. IC Chiralpak (25
185 cm × 4.6 mm (i.d.)) (Daicel Chemical Ind, Ltd. Japan) (Shen and Okamoto, 2016).

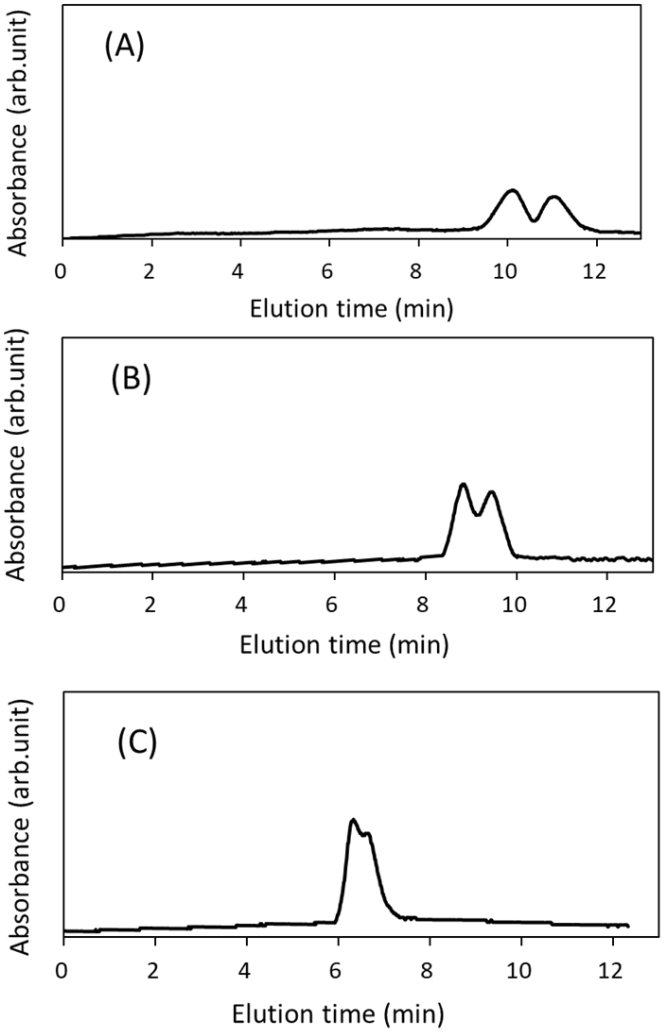

186

187 **Fig. 1.** Chromatogram when $[Co(acac)_3]$ (1×10^{-8} mole)) was eluted at (A) 4, (B) 15 and
188 (C) 30 ℃. The samples were injected as a volume of 50 μL. Flow rate was 0.2
189 $mLmin^{-1}$. The elution was monitored by electronic absorbance at 300 nm.

190

191 Separation behavior was examined by changing elution conditions such as
192 temperature, flow rates and injected amounts. Curves (A(, (B) and (C) in Figure 1
193 compare the chromatograms when the temperature changed from 4, 15 and 30 ℃,
194 respectively. On raising temperature, elution volumes decreased with the increase of

195 overlapping of two peaks. A corrected elution volume, (V_i - V_d) (i = 1 and 2), is related
196 to the thermodynamic parameters of the adsorption equilibrium as below:

197 $$\ln (V_i - V_d) = \Delta H/RT - \Delta S/R, \quad (2)$$

198 in which R, ΔH and ΔS are gas constant, the enthalpy and entropy changes of adsorption,
199 respectively. By plotting In (V_i -V_d) against 1/T (Fig. S5), ΔH and ΔS are calculated as
200 shown in Table 1. According to the results, Λ-[Co(acac)$_3$] is adsorbed by [Cu(*SS*-
201 oxa)]$^{2+}$/HEC stronger than Δ-[Co(acac)$_3$] with the larger enthalpy and smaller entropy
202 changes of adsorption.
203
204 **Table 1.** Thermodynamic parameters of adsorption of Δ- or Λ-[Co(acac)$_3$] on a column
205 of [Cu(*SS*-oxa)]$^{2+}$/HEC.

	Δ–[Co(acac)$_3$]	Λ-[Co(acac)$_3$]	difference
ΔH kJmol^{-1}	17.27	17.40	0.13
ΔS JK^{-1}mol^{-1}	- 44.02	- 43.78	- 0.24

206
207 Figures 2 (A), (B) and (C) show the chromatograms when [Co(acac)$_3$] (1 8 × 10^{-8}
208 mole) was eluted at the flow rates of 0.1, 0.2 and 0.3 mLmin^{-1}, respectively. The samples
209 were injected as a volume of 50 μL. On raising a flow rate, two peaks were more
210 overlapped until they were fused nearly to one broad band. According to the results in
211 Figure 2 (C), the time required for attaining adsorption equilibration (denoted as t_p) was
212 larger than the time for an injected molecule to pass through the column at the flow rate
213 of 0.3 mLmin^{-1}. From the dead volume of the column (1.65 mL) and the flow rate value,
214 t_p was estimated to be larger than 5 minutes.

215

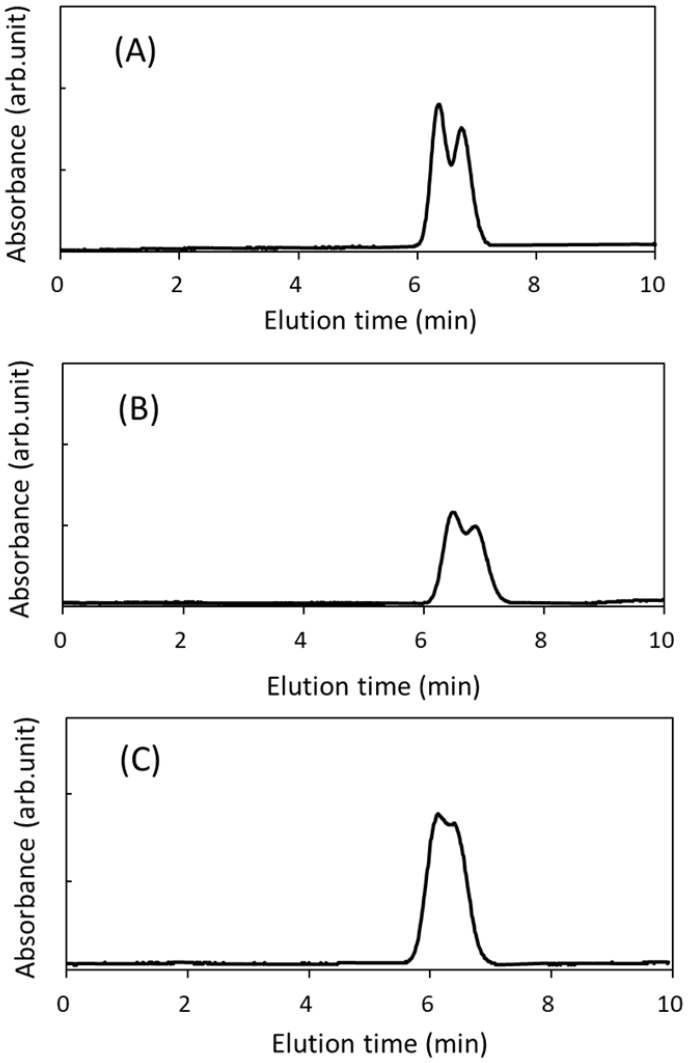

216

217 **Fig. 2.** Chromatogram when [$Co(acac)_3$] was eluted at 30 ℃ at the flow rate of
218 (A) 0.1, (B) 0.2 and (C) 0.3 $mLmin^{-1}$. Elution was monitored by the
219 electronic absorbance at 300 nm.

220

221 Figures 3 (A), (B) and (C) show the chromatograms when [$Co(acac)_3$] was eluted
222 at the injected amounts of 1.0×10^{-7}, 1.0×10^{-6} and 1.6×10^{-6} mole, respectively. The
223 flow rate was 0.2 $mLmin^{-1}$ and temperature 30 ºC. An injected volume was 50 μL. On

raising the injected amount, two peaks were overlapped until they were fused to one broad band. Thus the maximum amount of mounted [Co(acac)$_3$] (denoted by M_{max}) was 1.0×10^{-7} mole for two peaks to appear separately in the chromatogram. The amount of pre-adsorbed [Cu(*SS*-axo)]$^{2+}$ complexes was 1.5×10^{-3} mole. This was much larger than M_{max}. Thus only a small part of pre-adsorbed [Cu(*SS*-axo)]$^{2+}$ complexes were effective for resolution. Probably most of [Cu(*SS*-axo)]$^{2+}$ complexes were present within the inner parts of HEC particles so that they were unable to be contact with eluted [Co(acac)$_3$]. It will be important to identify the location of adsorbed [Cu(*SS*-oxa)]]$^{2+}$ within a clay material (HEC). It is proposed to apply the solid state NMR to discriminate between the Cu(II) complexes on an external surface and in the interlayer space. The chemical shift of peaks assigned to C^{13} atoms in [Cu(*SS*-oxa)]$^{2+}$ is expected to give the information on its location.

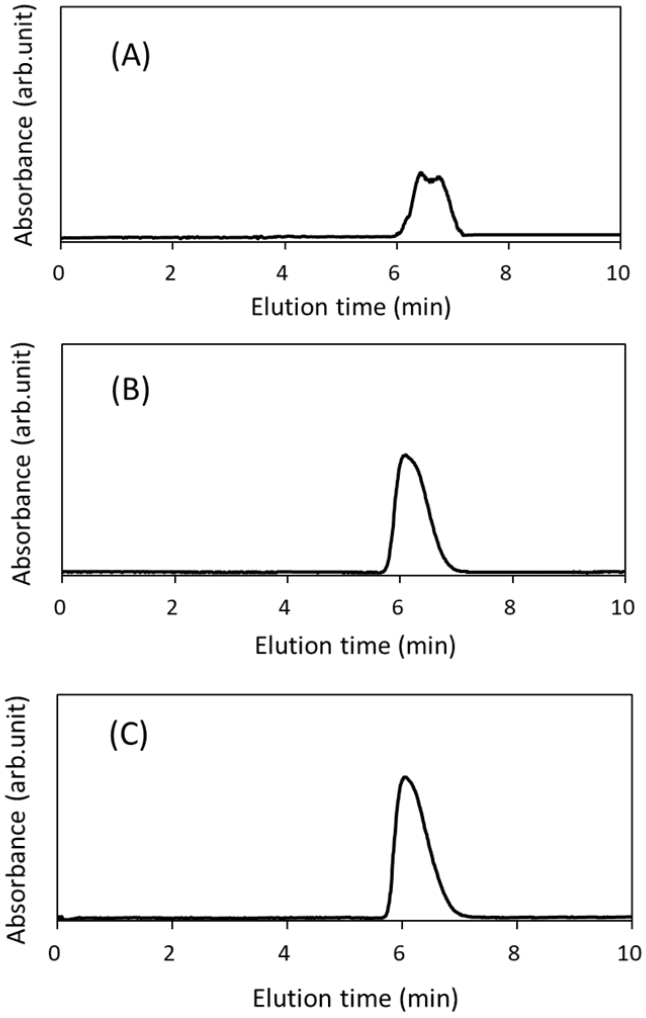

236

237 **Fig. 3.** Chromatogram when $[Co(acac)_3]$ was eluted when the injected amount was
238 changed from (A) 1.0×10^{-7}, (B) 1.0×10^{-6} and (C) 1.6×10^{-6} mole. The flow rate
239 was 0.2 mL min^{-1} and the temperature was 30 ˚C. Elution was monitored by
240 electronic absorbance at 300 nm.

241

242 Chromatographic behavior was compared for a series of tris(acetylacetonato)
243 metal(III) complexes (or $[M(acac)_3]$: M = Cr, Ir, Ru and Rh). The complexes were eluted
244 at 4 ℃ and a flow rate of 0.2 $mLmin^{-1}$. Figures 4 (A), (B), (C) and (D) show the

chromatograms of [Cr(acac)$_3$], [Ir(acac)$_3$], [Ru(acac)$_3$] and [Rh(acac)$_3$], respectively. The separation factor (α) is given in Table 2. From the table, α depended crucially on the kind of a central metal ion. [Co(acac)$_3$] (Figure 1 (A)) was resolved most efficiently. [Ir(acac)$_3$], [Ru(acac)$_3$] and [Rh(acac)$_3$] were partially resolved. [Cr(acac)$_3$] was not resolved to the detectable level by means of ECD measurements. From the ECD spectra of the fractions before and after the peak positions, elution order was from Δ to Λ for [M(acac)$_3$] (M = Co, Ir, Ru and Rh). Table 1 includes the ionic radius of a three-valent central metal ion (or M(III)). Based on these, [Co(acac)$_3$] is the smallest in size. This might be the reason that [Co(acac)$_3$] was resolved at highest separation factor. Alternatively it is suggested that there exists a cavity around [Cu(*SS*-axo)], whose size matches with [Co(acac)$_3$]. Other complexes were difficult to be resolved because they were too bulky to enter the cavity completely. [Cr(acac)$_3$] was not resolved in spite of its size smaller than that of [M(acac)$_3$] (M = Ir, Ru and Rh). One reason might lie in the high spin multiplicity of Cr(III) (or S = 3/2). Since Cu(II) has a spin of 1/2, it is suspected that the magnetic repulsion between Cr(III) and Cu(II) inhibited the occurrence of effective chiral discrimination.

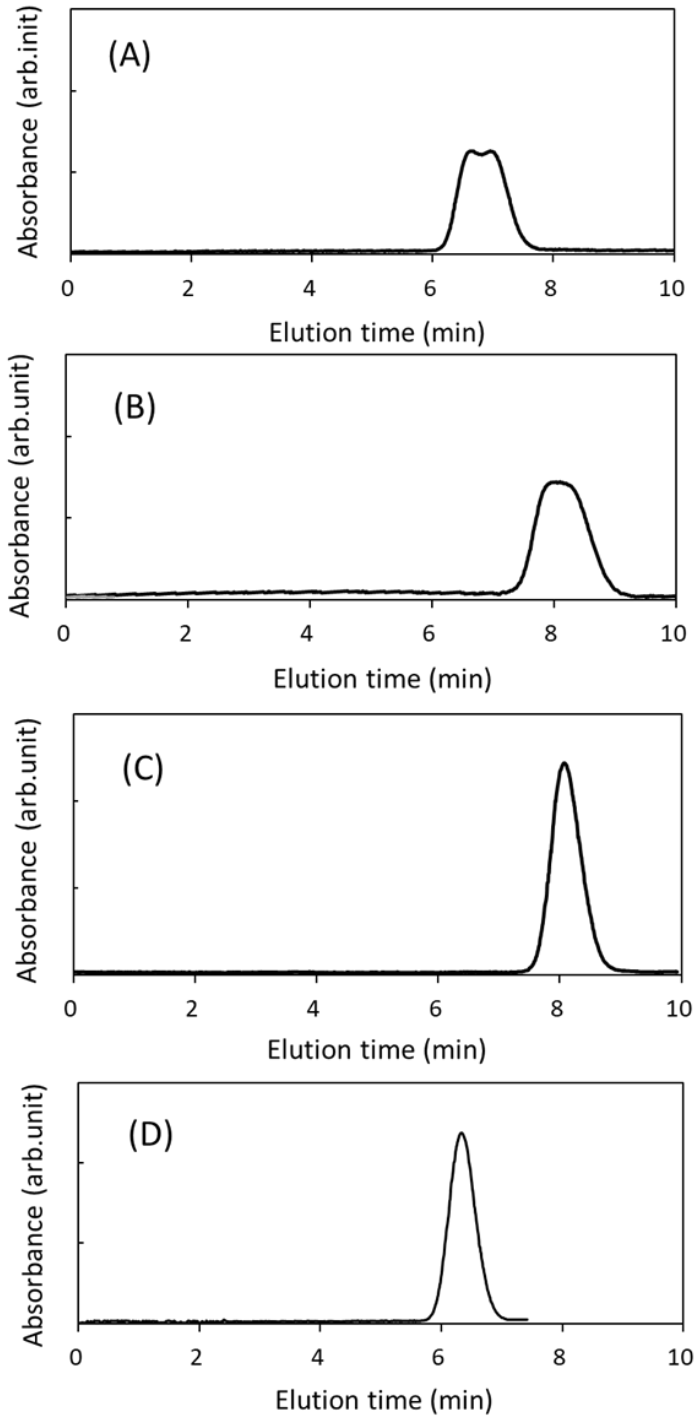

262

263 **Fig. 4.** Chromatogram when [$M(acac)_3$] was at the flow rate of 0.2 $mLmin^{-1}$ and

264 temperature 4 ºC. The injected amount was 1.0×10^{-7} for all runs. Elution was

monitored by electronic absorbance at 330 nm, (A) [Ir(acac)$_3$]), 320 nm; (B) [Ru(acac)$_3$], 270 nm; Rh(acac)$_3$], 320 nm; [Cr(acac)$_3$], 330 nm, respectively.

Table 2. Chromatographic results for a series of [M(acac)$_3$]. The elution conditions are stated in the caption of Figure 4.**

Complex	V_1 -V_d (mL)	V_2 -V_d (mL)	Separation factor	Ionic radius (M^{3+}) (pm) *
[Ir(acac)$_3$]	5.03	5.38	1.07	82
[Ru(acac)$_3$]	6.19	6.6	1.07	82
[Rh(acac)$_3$]	6.33	6.58	1.04	81
[Cr(acac)$_3$]	4.73	4.73	1	76

*Cited from Shannon R. D. (1976) Act. Crystallogr. A32, 751.

** An error in estimating the elution volume was 5%.

In order to obtain a support for the existence of a microscopic cavity in [Cu(*SS*-axo)]$^{+2}$/HEC, the chromatographic behavior of [Co(acac)$_3$] was compared using a column packed with [Cu(*SS*-axo)(dbm)]$^{+}$/HEC (5 cm x 0.4 cm (i.d.)). In this column, a vacant space around Cu(II) ion was already occupied by dbm^{-}. On this column, [Co(acac)$_3$] was eluted nearly at the volume close to V_d (dead volume: 0.35 mL) (not shown). The results supported that an empty space around a Cu(II) ion in [Cu(*SS*-axo)]$^{2+}$/HEC acted as a microscopic cavity for recognizing the chirality of an eluted molecule.

Resolution of chiral organic molecules: In order to extend the scope of targets, a number of chiral organic molecules were eluted on the present column. There have been several

columns developed for resolving organic molecules chromatographically (Wang et al., 2023; Hoyas et al., 2021; Wahab et al., 2017; Shen and Okamoto, 2016). For the purpose, *S*-, *R*- and racemic 1,1'-bibaphthyl-2,2'-diols (denoted as *R*-, *S*- and rac-BINAL, respectively) were eluted. BINAL possesses two helically twisted phenyl groups (Chart 2). The molecule was anticipated to interact with the two phenyl groups of $[Cu(SS\text{-oxa})]^{2+}$ through π–π interactions. Figures 5 (A), (B) and (C) show the chromatograms when racemic, *R*- and *S*-BINAL (1 x 10^{-8} mol) were eluted at 30 °C and a flow rate of 0.2 $mLmin^{-1}$, respectively. In case of (A), two peaks appeared. They were partially overlapped. The ECD spectra of the solutions collected at the first and second peaks showed that they contained *R*-BINAL and *S*-BINAL as an excess enantiomer, respectively. The results were consistent when *R*- and *S*-enantiomers were eluted separately ((B) and (C) in Figure 5, respectively).

(A) BINAL

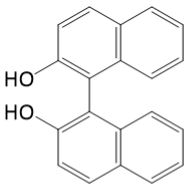

(B) BINAL-Br

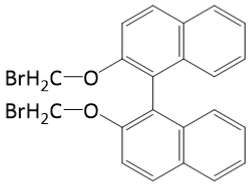

(C) 1-phenylethyl-1,2-diol

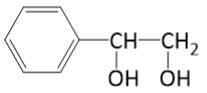

(D) 1-phenylethylalcohol

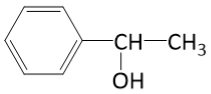

(E) 1-phenylethylamine

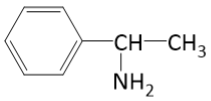

(F) 1,2-diphenylethane-1,2-diol

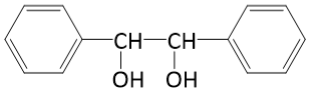

Chart 2. Molecular structures of (A) BINAL, (B) BINAL-Br, (C) 1-phenylethane-1, 2-diol, (D) 1-phenylethanol, (E) 1-phenylethyamine and (F) 1, 2-diphenylethane-1, 2-diol.

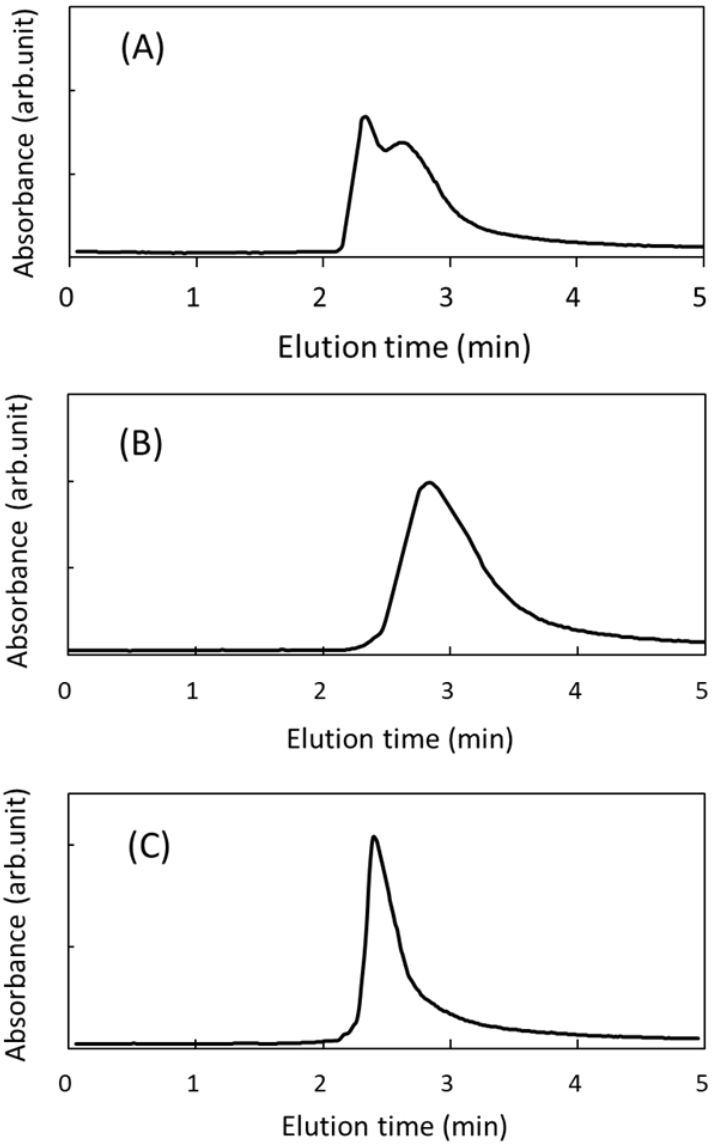

299

300 **Fig. 5.** Chromatograms when (A) racemic BINAL, (B) *R*-BINAL and (C) *S*-BINAL were
301 eluted at 30 ºC and a flow rate of 0.2 mLmin^{-1}. The injected amount was 1×10^{-8}
302 mole. The elution was monitored by electronic absorbance at 270 nm.

303

304 For comparison, 1,1'-bibaphthyl-2,2'-dibromomethoxy (BINAL-Br) (Chart 2) was
305 eluted under the same conditions. The chromatogram showed one single band nearly at

306 the dead volume (or at 1.80 mL) (not shown). The ECD spectra of the solutions collected
307 at the former and latter parts of the band showed no ECD activity. Thus BINAL-Br
308 showed no affinity towards the column. It was suspected that the presence of OH groups
309 were necessary for a molecule to be resolved by the column. One possibility was that the
310 two OH groups in BINAL coordinated weakly a Cu(II) ion in $[Cu(SS\text{-oxa})]^{2+}$, while no
311 such interaction was possible in case of BINAL-Br.

312 Prompted by the above hypotheses, other compounds with one or two OH groups
313 were eluted. The results are summarized in Table 3. As a result, 1-phenylethane-1,2-diol
314 was resolved partially, validating the hypothesis. When 1-phenylethylamine was mounted,
315 it was not eluted at all. It indicated that the amino group in the molecule coordinated
316 strongly with a Cu(II) ion in the column.

317

318 **Table 3.** Chromatographic results for organic compounds. The elution conditions were
319 the same as in Figure 5.

Compound	$V_1 - V_d$ (mL)	$V_2 - V_d$ (mL)	separation factor
1,1'-bibaphthyl-2,2'-diol	0.53	0.93	1.76
1,1'-bibaphthyl-2,2'-dibromomethoxy	0.02	0.02	1
1-phenylethyl-1,2-diol	1.40 (S)	1.73 (R)	1.24
1-phenylethanol	0.5	0.5	1
1-phenylethylamine	Not eluted	Not eluted	
1, 2-diphenylethane-1, 2-diol	1.17 (SS)	1.25 (RR)	1.07

320 (*) An error in estimating the elution volume was 5%.

Theoretical simulation for the binding of [Co(acac)$_3$] on the column: the binding of Δ- or Λ-[Co(acac)$_3$] on the column packed with [Cu(SS-oxa)]$^+$/HEC was studied theoretically. The simulated system contained Δ- or Λ-[Co(acac)$_3$], [Cu(SS-oxa)]$^+$ and one SiO_4^{2-} anion. Here, SiO_4^{2-} was included in the place of a clay layer to maintain the condition of charge neutrality.

Figures 7 (A) and (B) show the optimum structures when the Δ- and Λ-enantiomers of [Co(acac)$_3$] are associated with [Cu(*SS*-oxa)]$^{2+}$ in the presence of SO_4^{2-}. Both of the enantiomers are located close to a central Cu(II) ion. The Co(III) – Cu(II) distance is 0.32 and 0.31 nm, respectively. Two phenyl groups in [Cu(*SS*-oxa)]$^{2+}$ orient so as to surround the enantiomers. One remarkable difference is that the angle between the phenyl groups for a pair of Δ-[Co(acac)$_3$]/[Cu(*SS*-oxa)]$^{2+}$is large (< 150 degree) for the Δ-enantiomer, while it is small (> 110 degree) for the Λ-enantiomer. This implies that the steric hindrance is larger for a pair of Δ-[Co(acac)$_3$]/[Cu(*SS*-oxa)]$^{2+}$ than for a pair of Λ-[Co(acac)$_3$]/[Cu(*SS*-oxa)]$^{2+}$. This leads to the lower stabilization energy for the former pair than for the latter pair. In fact, the stabilization energy in Λ-[Co(acac)$_3$]/[Cu(*SS*-oxa)]$^{2+}$ is calculated to be lower by 15.7 kJmol^{-1} than that in Δ-[Co(acac)$_3$]/[Cu(*SS*-oxa)]$^{2+}$.Thus the calculation predicts that the Λ-enantiomer binds with [Cu(*SS*-oxa)]$^{2+}$ stronger than the Δ-enantiomer. This is in accord with the experimental results. The calculation implied that the stabilization was achieved by the "induced-fit" of the two phenyl moieties in [Cu(SS-oxa)]$^{2+}$ when Λ-[Co(acac)$_3$] entered the cavity around a Cu(II) ion. No such "induced-fit" took place in case of Δ-[Co(acac)$_3$].

(A)

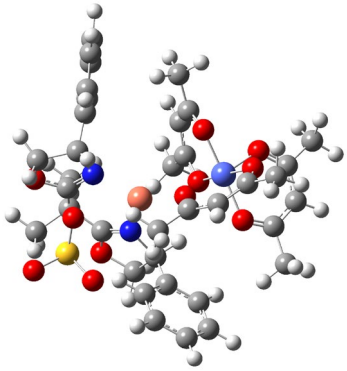

(B)

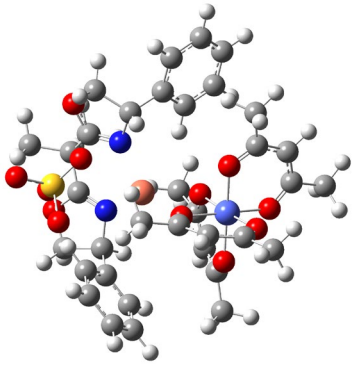

Fig. 6. The optimum structures of enantiomeric $[Co(acac)_3]$ associated with $[Cu(SS\text{-}oxa)]^{2+}$ in the presence of SO_4^{2-}; (A) Δ-$[Co(acac)_3]$/$[Cu(SS\text{-}oxa)]^{2+}$ and (B) Λ-$[Co(acac)_3]$/$[Cu(SS\text{-}oxa)]^{2+}$.

4. Conclusions

Chromatographic resolution was performed by use of a column packed with an ion-exchange adduct of synthetic hectorite and a chiral Cu(II) complex. The used chiral

complex was $[Cu(SS\text{-oxa})]^{2+}$ (*SS*-oxa=*SS*-2,2′-isopropylidene-bis(4-phenyl-2-oxazoline)). The column resolved a racemic mixture of $[Co(acac)_3]$ (acacH = acetylacetone) to Δ- and Λ-enantiomers nearly to the baseline separation. With the help of theoretical simulation, it was concluded that the resolution was realized by the occupation of the enantiomers in a cavity around a Cu(II) ion. As for organic compounds, the column exhibited the resolution ability toward an organic molecule with two hydroxyl groups. It was suggested that the molecule binds with a Cu(II) ion in a stereoselective way through coordinating interactions.

Author Contributions

All authors contributed equally.

Conflicts of interest

There are no conflicts to declare.

Acknowledgements

This work was financially supported by the Japan Society for the Promotion of Science (JSPS) KAKENHI Grant (JP22H02033, JP22K0526 and JP20K21090). The computations were performed in collaboration with the Research Centre for Computational Science, Okazaki, Japan (Project:23-IMS-C160).

References

Fraile, J. M., García, J. I., Mayoral, J. A., 2009. Noncovalent immobilization of enantioselective catalyst. Chem. Rev. 109, 360-417. https://doi.org/10.1021/cr800363y

Frisch, M.J., Trucks, G.W., Schlegel, H.B., Scuseria, G.E., Robb, M.A., Cheeseman, J.R., Scalmani, G., Barone, V., Petersson, G.A., Nakatsuji, H., Li, X., Caricato, M., Marenich, A.V., Bloino, J., Janesko, B.G., Gomperts, R., Mennucci, B., Hratchian, H. P., Ortiz, J.V., Izmaylov, A.F., Sonnenberg, J.L., Williams-Young, D., Ding, F., Lipparini, F., Egidi, F., Goings, J., Peng, B., Petrone, A., Henderson, T., Ranasinghe, D., Zakrzewski, V.G., Gao, J., Rega, N., Zheng, G., Liang, W., Hada, M., Ehara, M., Toyota, K., Fukuda, R., Hasegawa, J., Ishida, M., Nakajima, T., Honda, Y., Kitao, O., Nakai, H., Vreven, T., Throssell, K., Montgomery, J.A.J., Peralta, J.E., Ogliaro, F., Bearpark, M.J., Heyd, J.J., Brothers, E.N., Kudin, K.N., Staroverov, V.N., Keith, T.A., Kobayashi, R., Normand, J., Raghavachari, K., Rendell, A.P., Burant, J. C., Iyengar, S.S., Tomasi, J., Cossi, M., Millam, J.M., Klene, M., Adamo, C., Cammi, R., Ochterski, J.W., Martin, R.L., Morokuma, K., Farkas, O., Foresman, J.B., Fox, D.J., 2019. Gaussian 16, Revision C.02.

Hoyas, S., Roscioni, O. M., Tonneaux, C., Gerbaux, P., Cornil, J., Muccioli, L., 2021. Peptoids as a chiral stationary phase for liquid chromatography: Insights from molecular dynamics simulations. Biomacromolecules, 22, 2573−2581. https://doi.org/10.1021/acs.biomac.1c00302

Johnson. J. S., Evans. D. A., 2000. Chiral bis(oxazoline) copper(II) complexes: Versatile catalysts for enantioselective cycloaddition, aldol, michael, and

carbonylene reactions. *Acc. Chem. Res.*, 2000, **33**, 325–335. https://doi.org/10.1021/ar960062n

Kakegawa, N., Yamagishi, A., 2005. Coadsorption studies of tris(1,10-phenanthroline) ruthenium(II) and N-methylated alkaloid cation by laponite with an application for a chiral column packing material. Chem. Mater., 17, 2997-3003. https://doi.org/10.1021/cm048285s

Kotkar, D. Ghosh, D. P., 1987. Effect of pH on the chromatographic resolution of carboxy derivatives of tris(bipyridyl)ruthenium(II) on a chirally modified montmorillonite column. Inorg. Chem. 26, 208-209. https://doi.org/10.1021/ic00248a041

Ogawa, M., Kuroda, K., 1995. Photofunctions of intercalation compounds. Chem. Rev. 95, 399-438. https://doi.org/10.1021/cr00034a005

Okada, T., Mutsuki, O., Tajima, K., Yamakami, T., Hisako Sato, H., 2018. Variation in thickness of a layered silicate on spherical silica particles affected HPLC chiral chromatographic resolution. Appl. Clay Sci., 163, 72-80. https://doi.org/10.1016/j.clay.2018.07.017

Sakuma, K., Tamura, K., Minagawa, K., 2018. “Doughnut”-like clay microparticles fabricated using a hybrid method of spray drying and centrifugal disc atomization. Chem. Lett., 47, 68-70. https://doi.org/10.1246/cl.170891

Sato, H., Tamura, K., Takimoto, K., Yamagishi, A., 2018a. Solid state vibrational circular dichroism towards molecular recognition: Chiral metal complexes intercalated in a clay mineral. Phys. Chem. Chem. Phys. 20, 3141-3147. https://doi.org/10.1039/c7cp05114j

421 Sato, H. Takimoto, K., Mori, H., Yamagishi, A., 2018b. Stereoselective interactions as
422 manifested by vibrational circular dichroism spectra: Interplay between chiral
423 metal complexes Co-adsorbed in a montmorillonite clay. Phys. Chem. Chem.
424 Phys. 20, 25421-25427. https://doi.org/10.1039/c8cp04753g
425 Sato, H. Takimoto, K., Yoshida, J., Yamagishi, A., 2020. Vibrational circular dichroism
426 towards asymmetric catalysis: Chiral induction in substrates coordinated with
427 copper(II) Ions. Phys. Chem. Chem. Phys. **22,** 24393-24398.
428 https://doi.org/10.1039/d0cp04827e
429 Sato, H., Takimoto, K., Yoshida, J., Watanabe, Y., Yamagishi, A., 2021. Solid-state
430 vibrational circular dichroism as applied for heterogenous asymmetric catalysis:
431 Copper (II) complexes immobilized in montmorillonite. Chem. Lett. 50, 896-898.
432 https://doi.org/10.1246/cl.200937
433 Sato, H., Takimoto, K., Yamagishi, A., Yoshida, J., Hara, M., 2022. Vibrational circular
434 dichroism spectroscopy toward intercalation compounds of sodium
435 montmorillonite: evidences for molecular packing of enantiopure monovalent
436 Ir(III) complexes within interlayer spaces. Appl. Clay Sci., 228, 106621.
437 https://doi.org/10.1016/j.clay.2022.106621
438 Schoonheydt, R. A., 2014. Functional hybrid clay mineral films. Appl. Clay Sci. 96, 9-
439 21. https://doi.org/10.1016/j.clay.2014.04.010
440 Shannon, R. D., 1976. Revised effective ionic radii and systematic studies of
441 interatomic distances in halides and chalogenides. Acta Cryst. A32, 751-767.
442 https://doi.org/10.1107/S0567739476001551
443 Shen, H., Okamoto, Y., 2016. Efficient separation of enantiomers using stereoregular

chiral polymers. Chem. Rev., 116, 1094−1138.
https://doi.org/10.1021/acs.chemrev.5b00317

Shichi, T., Takagi, K., 2000. Clay minerals as photochemical reaction fields. J. Photochem. Photobiol. C: Photochem. Rev. 1, 113-130. https://doi.org/10.1016/S1389-5567(00)00008-3

Yamagishi, A. Soma, M.,1981. Optical resolution of metal chelates by use of adsorption on a colloidal clay. J. Am. Chem. Soc., 103, 4640-4642. https://doi.org/10.1021/ja00405a086

Yamagishi, A. Ohnishi, R. 1982. Clay column chromatography for optical resolution: Initial resolutions of bis(acetylacetonato)(glycinato)cobalt(III) and (acetylacetonato)bis(glycinato)cobalt(III) on a Δ-tris(1,10-phenanthroline) nickel(II)-montmorillonite column. Inorg. Chem. 21, 4233-4236. https://doi.org/10.1021/ic00142a024

Yamagishi, A. 1985. Chromatographic resolution of enantiomers having aromatic groups by an optically active clay-chelate adduct. J. Am. Chem. Soc. 107, 732-734. https://doi.org/10.1021/ja00289a051

Yamagishi, A.,1986. Optical resolution and racemization reaction of tris(bathophenanthrolinedisulfonato)iron(II): Absence of an intramolecular racemization path in aqueous solution. Inorg. Chem. 25, 55-57. https://doi.org/10.1021/ic00221a015

Yamagishi, A., Makino, H., Nakamura, Y., Sato, H., 1992. Separation of isomers of cobalt(III) complexes by liquid chromatography on a column packed with a clay,

ruthenium(II) complex adduct.Clay. Clay Miner. 40, 359-361. https://doi.org/10.1346/CCMN.1992.0400318

Yamagishi, A., Taniguchi, M., Imamura, Y., Sato, H., 1996. Clay column chromatography for optical resolution: Selectivities of L-$[Ru(phen)_3]^{2+}$ and L-$[Ru(bpy)_3]^{2+}$ Laponite columns toward 1,1'-binaphthol. Appl. Clay Sci. 11, 1-10. https://doi.org/10.1016/0169-1317(96)00010-5

Yamagishi, A., Sato, H., 2012. Stereochemistry and molecular recognition on the surface of a smectite clay mineral. Clay. Clay Miner. 60, 411-419. https://doi.org/10.1346/CCMN.2012.0600407

Yamagishi, A. Takimoto, K., Tamura, K., Sato, F., Sato, H., 2021. Chiral discrimination of dansylated alanine methyl ester on a modified clay surface: vibrational circular dichroism approach. Bull. Chem. Soc. Jpn., 94, 2711-2717. https://doi.org/10.1246/bcsj.20210291

Yamagishi, A., Yamamoto, S., Takimoto, K., Tamura, K., Kamon, M., Sato, F., Sato, H., 2022. Clay column chromatography for optical resolution: a series of derivatized amino acids. Bull. Chem. Soc. Jpn., 95, 961–967. https://doi.org/10.1246/bcsj.20220077

Yoshida, J., Tateyama, K., Kasahara, Y., Yuge, H., 2020a. Stabilization of oxidized ruthenium complexes by adsorption on clay minerals. App. Clay Sci. 199, 1, 105869. https://doi.org/10.1016/j.clay.2020.105869

Yoshida, J., Tateyama, K., Yuge, H., Hara, M., 2020b. Hexagonal ordering of racemic Ni(II) complexes in the interlayer space of a clay mineral. Chem. Commun. 56, 10670-10673. https://doi.org/10.1039/D0CC04977H.

Wahab, M. F. Patel, D. C., Wimalasinghe, R. M., Armstrong, D. W., 2017. Fundamental and practical insights on the packing of modern high efficiency analytical and capillary column. Anal. Chem. 89, 8177−8191. https://doi.org/10.1021/acs.analchem.7b00931

Wang, F., Li, X., Jiang, S., Han, J., Wu, J., Yan, M., Yao, Z., 2023. Enantioselective behaviors of chiral pesticides and enantiomeric signatures in foods and the environment. J. Agric. Food Chem. 71, 12372−12389. https://doi.org/10.1021/acs.jafc.3c02564

Supporting Information

Use of an Ion-exchange Adduct of Synthetic Hectorite and Chiral Copper(II) Complex as a Packing Material for Chromatographic Resolution

Akihiko Yamagishi,[a] *Kenji Tamura,**[b] *Masumi Kamon,*[b] *Jun Yoshida* [c] *and Hisako Sato**[d]

[a] Toho University, School of Medicine, Ohta-ku, Tokyo 143-8540, Japan

[b] National Institute for Materials Science, Environmental Circulation Composite Materials Group, Tsukuba, 305-0044, Japan

[c] Nihon University, Department of Chemistry, College of Humanities & Sciences, Setagaya-ku, Tokyo 156-8550, Japan

[d] Ehime University, Department of Chemistry, College of Science, Matsuyama, Ehime 790-8577, Japan,

*Corresponding author: Kenji Tamura (TAMURA.Kenji@nims.go.jp)

Tel: +81-29-860-4370, Fax: +81-29-860-4667

Contents

Fig. S1. The electronic circular dichroism spectra (ECD) of 1,1'-binaphthyl-2, 2'-dibromomethoxy (denoted as BINAL-Br). BINAL-Br was synthesized in our laboratory. The purity of the compound was checked by eluting on a chiral column (RU-1 Ceramosphere (Shiseido Ind. Co.)). Two separate peaks were obtained. The ECD spectra of the first and second peaks are shown below. The mirror image relation was obtained to confirm their purity.

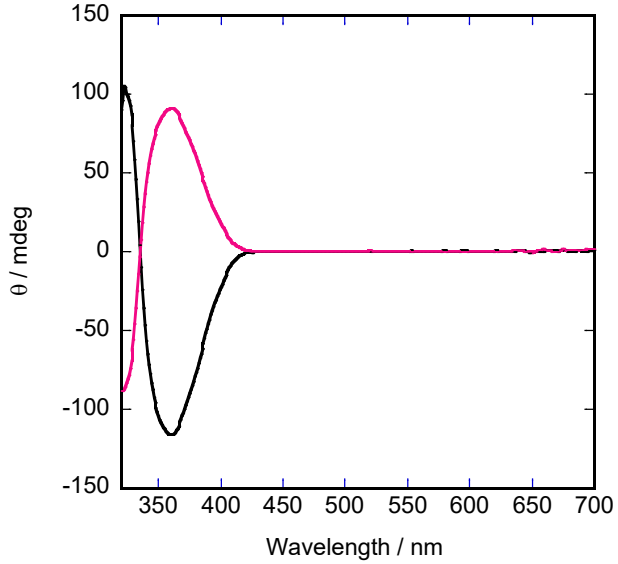

Figure S1. The ECD spectra of the first (black) and second fractions (red) of eluted BINAL-Br. The first and second fractions were corresponded to *R*- and *S*-enantiomers, respectively.

564

565 **Fig S2.** Curves of nitrogen adsorption−desorption isotherms for Laponite particles: (open
566 circles) adsorption profile and (solid circles) desorption profile. Based on the results,
567 **Table. S1** lists the BET surface area ($A_{s,BET}$) and pore volume (V_p).

568

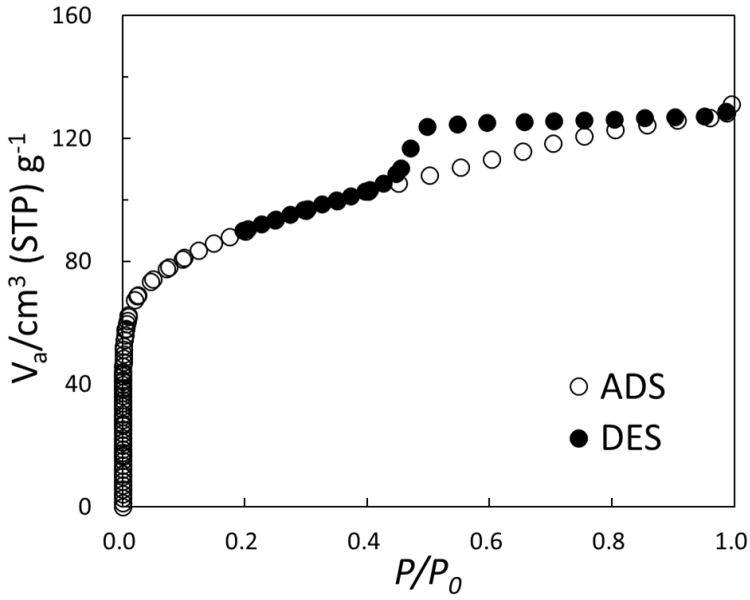

569

570 **Figure S2.** Curves of nitrogen adsorption−desorption isotherms for Laponite particles:
571 (open circles) adsorption profile and (solid circles) desorption profile.

572

573 **Table S1.** BET surface area (A_s) and the total pore
574 volume (V_p) of Laponite particles.

$A_{s,\ BET}$	320	($m^2\ g^{-1}$)
V_p	0.14	($cm^3\ g^{-1}$)

575

576

577 **Fig S3**. XRD patterns of (a) Laponite particles (or Na-HEC) and (b) [Cu(*SS*-
578 oxa)]$^{2+}$/Laponite particles (or [Cu(*SS*-oxa)]$^{2+}$/HEC), respectively. The weak peak
579 observed around 2θ~60.8° corresponds to the (060) reflection with a *d*-spacing of 0.15
580 nm, indicating trioctahedral smectite. The basal spacing, *d(001)*, was determined to be (a)
581 1.3 nm and (b) 1.43 nm, respectively. From the results, the basal spacing expanded by c.a.
582 0.13 nm. Moreover the sharpening of the peak (001) implied that the improvement of
583 ordering of layer stacking on the adsorption of [Cu(*SS*-oxa)]$^{2+}$ ions.

584

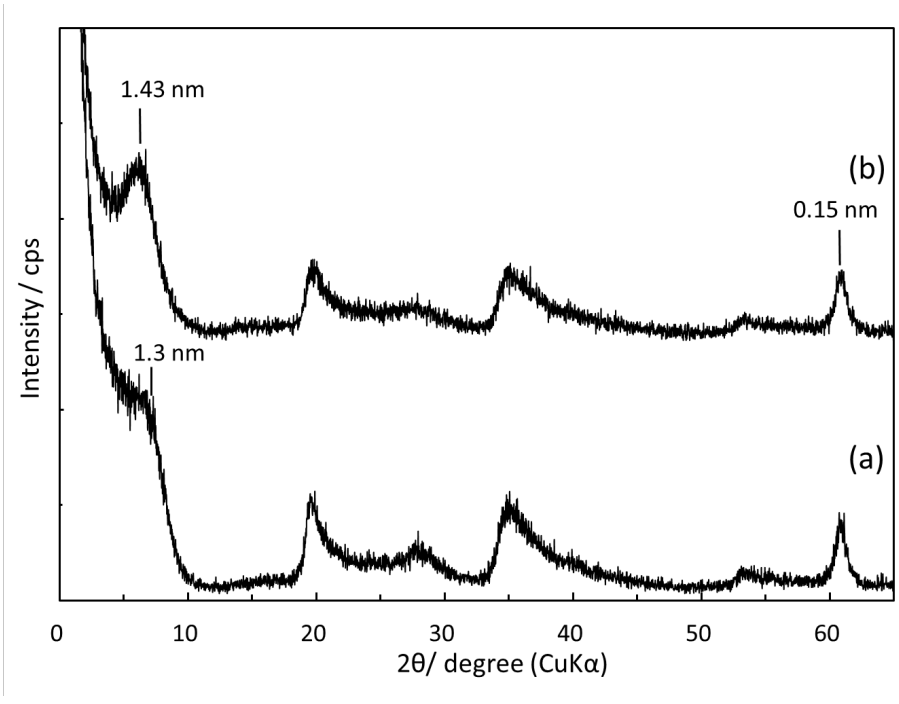

585

586 **Figure S3.** XRD patterns of (a) Laponite particles (or Na-HEC) and (b) [Cu(*SS*-
587 oxa)]$^{2+}$/Laponite particles (or [Cu(*SS*-oxa)]$^{2+}$/HEC), respectively.

588

589

590 **Fig S4.** SEM images of particles for (a)/(b) Na-HEC and (c)/(d) [Cu(*SS*-oxa)]$^{2+}$/HEC,
591 respectively. The images indicated that the particle maintained a spherical shape after
592 adsorbing [Cu(*SS*-oxa)]$^{2+}$.

593

594

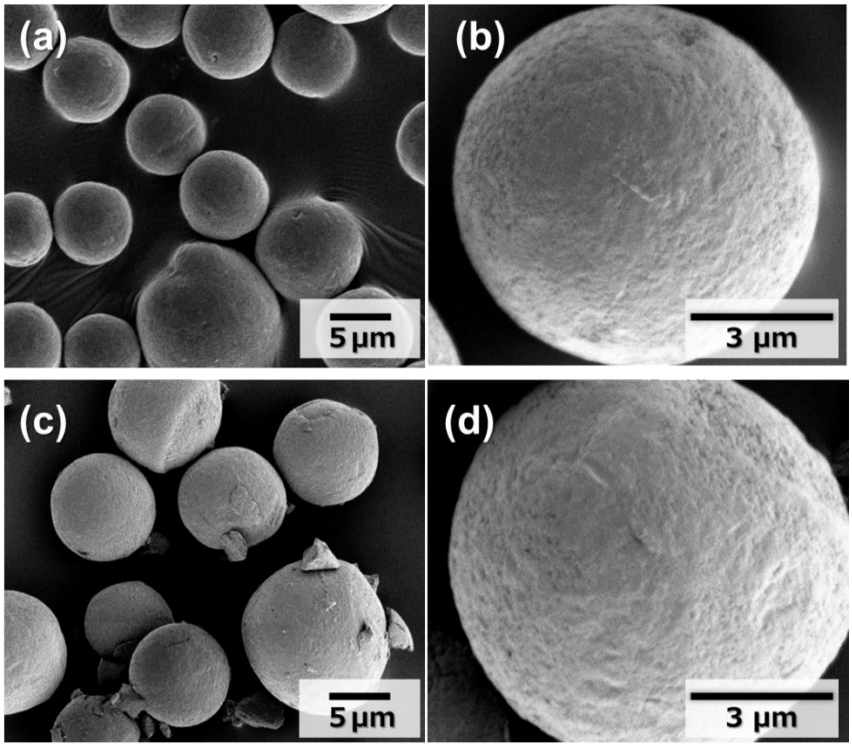

595

596 **Figure S4.** SEM images of particles for (a)/(b) Na-HEC and (c)/(d) [Cu(*SS*-
597 oxa)]$^{2+}$/HEC.

598

599

Fig S5. The Arrhenius plots of the natural logarithm of the elution volume versus the reciprocal of temperature. The plot gives the thermodynamic parameters of adsorption equilibrium as below:

$$\mathbf{In\ (V_i - V_d) = \Delta H/RT - \Delta S/R}$$

in which R, **Δ**H and **Δ**S are gas constant, the enthalpy and entropy changes of adsorption, respectively.

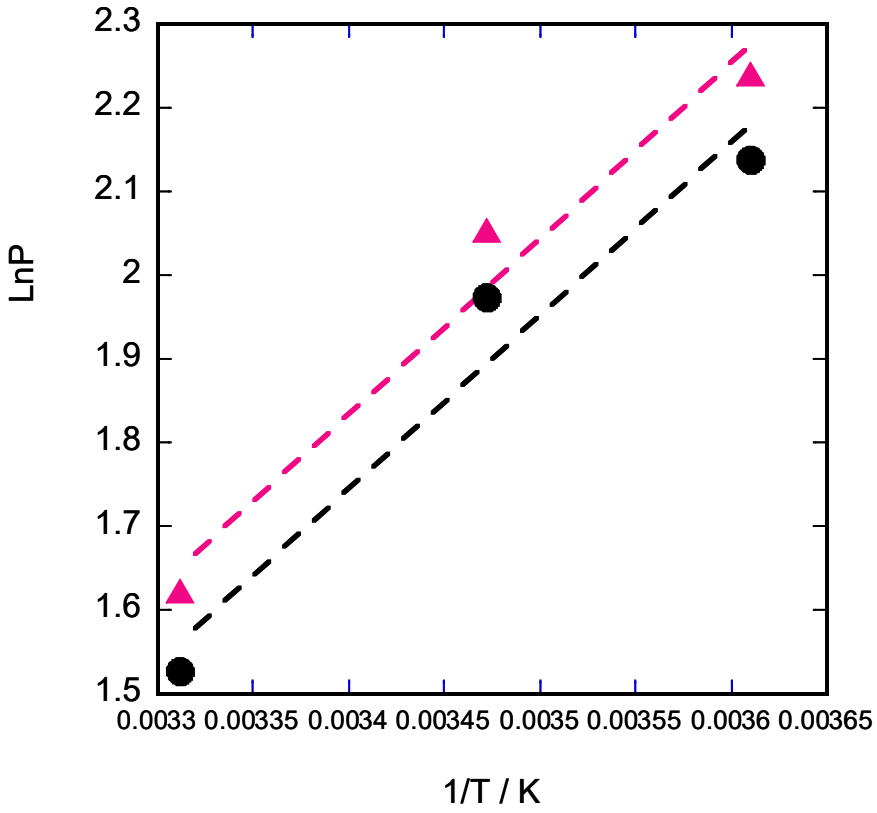

Figure S5. The Arrhenius plots of the natural logarithm of elution volume versus the reciprocal of temperature: filled black circles (peak 1) and red triangles (peak 2). The data are taken from the temperature dependence of the elution chromatogram of $[Co(acac)_3]$ (Figure 1 in the text).